Inorganic Chemistry

Article

pubs.acs.org/IC

Syntheses, Structures, and Magnetic Properties of seven-coordinate Lanthanide Porphyrinate or Phthalocyaninate Complexes with Kläui's Tripodal Ligand

Feng Gao,[†] Min-Xia Yao,[‡] Yu-Yang Li,[†] Yi-Zhi Li,[†] You Song,*[,†] and Jing-Lin Zuo*[,†]

[†]State Key Laboratory of Coordination Chemistry, School of Chemistry and Chemical Engineering, Nanjing National Laboratory of Microstructures, Nanjing University, Nanjing 210093, PR China

[‡]School of Science, Nanjing University of Technology, Nanjing 210009, PR China

Supporting Information

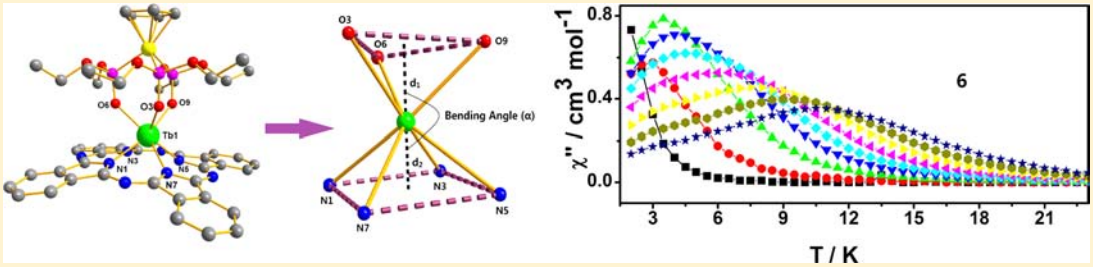

ABSTRACT: A series of seven-coordinate mononuclear lanthanide(III) complexes of the general formula $[(TPP)Ln(L_{OEt})]\cdot 0.25H_2O$ and $[(Pc)Ln(L_{OEt})]$ (Ln^{3+} = Dy^{3+}, Tb^{3+}, Ho^{3+}, and Gd^{3+}; TPP = 5,10,15,20-tetraphenylporphyrinate; Pc = phthalocyaninate; L_{OEt}^- = $[(\eta^5\text{-}C_5H_5)Co(P(=O)(OEt)_2)_3]^-$) are synthesized on the basis of the tripodal ligand L_{OEt}^- and either porphyrin or phthalocyanine ligands. All of the complexes are characterized by X-ray crystallography and by static and dynamic magnetic measurements. The Dy and Tb complexes show the field-induced slow relaxation of magnetization, and they are interesting seven-coordinate single-lanthanide-based SMMs. The magnetic relaxation properties of these double-decker sandwich complexes are influenced by the local molecular symmetry and are sensitive to subtle distortions of the coordination geometry of the paramagnetic lanthanide ions, such as metal-to-plane distances, plane center distances, and bending angles.

INTRODUCTION

Single-molecule magnets (SMMs) that exhibit slow relaxation of the magnetization below the blocking temperature (T_B) have attracted much interest in recent decades. This is not only because of the scientific point of view, such as quantum tunneling of magnetization and quantum phase interference, but also because of their potential applications, such as high-density magnetic storage, memory, sensors, quantum computing, and, more recently, spintronics.[1] For a SMM, it must possess a large overall ground-state spin quantum number (S) and a significant uniaxial magnetoanisotropy (negative zero-field-splitting parameter, D) that cause the formation of an energy barrier (U), preventing the reversal of the molecular magnetization. So far, many first-row transition metal ion-based SMMs have been reported.[2,3] In comparison to the transition-metal ions, lanthanide and actinide ions usually exhibit a large ground-state spin and a strong easy-axis magnetic anisotropy that can be used to construct SMMs containing higher effective energy barriers.

Recently, some rare-earth SMMs have been reported.[4] Among them, single rare-earth ion systems that can also exhibit a slow relaxation of the magnetization were first observed by Ishikawa et al. for mononuclear lanthanide complexes with either phthalocyanine or polyoxometalate ligands.[5−7] For these SMMs, the slow relaxation of the magnetization is mainly influenced by the interaction between the single-ion electron density and the crystal field environment in which it is placed.[8] So the crystal field is very important for constructing SMMs with single rare-earth ions.

In our previous work, a series of seven-coordinate mononuclear lanthanide complexes based on the chiral N_2O_2 coordination mode of salen-type ligands and Kläui's tripodal ligand, $[(\eta^5\text{-}C_5H_5)Co\{P(=O)(OEt)_2\}_3]^-$ (L_{OEt}^-, Scheme 1, right) were synthesized to study their magnetic properties.[9] In this Article, the more rigid macrocyclic tetradentate ligands porphyrin and phthalocyanine (Scheme 1, left and middle) and the tripodal ligand L_{OEt}^- are reacted with different lanthanide ions to prepare more seven-coordinate mononuclear lanthanide complexes, and to investigate the relationship between the magnetic properties and the crystal field coordination environment that results from the different tetradentate ligands. Additionally, when compared to salen-type ligands the coordination of the rigid macrocyclic ligands with localized electron pairs to lanthanide may generate higher uniaxial local symmetry. In this Article, eight new seven-coordinate

Received: January 31, 2013
Published: May 21, 2013

   dx.doi.org/10.1021/ic400245n | Inorg. Chem. 2013, 52, 6407−6416

Scheme 1. Ligands Used in This Work

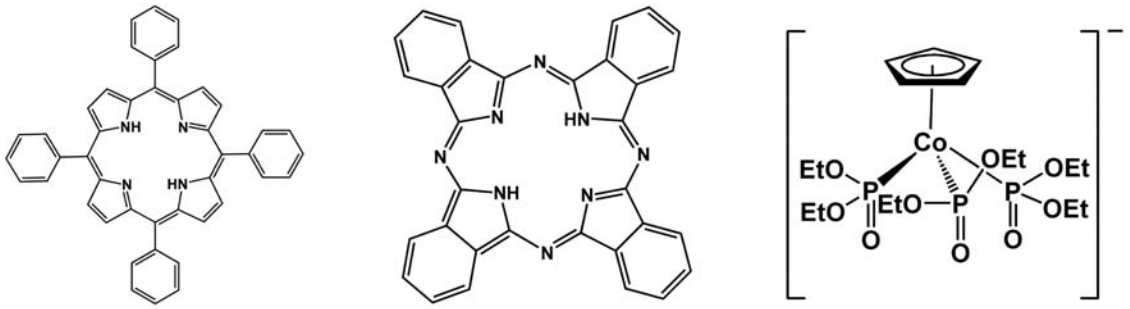

H_2TPP H_2Pc L_{OEt}^-

mononuclear complexes of the tripodal ligand L_{OEt}^- and either the porphyrinate or the phthalocyaninate ligand with paramagnetic lanthanide ions are synthesized: $[(L_{OEt})Dy(TPP)]\cdot 0.25H_2O$ (**1**), $[(L_{OEt})Tb(TPP)]\cdot 0.25H_2O$ (**2**), $[(L_{OEt})Ho(TPP)]\cdot 0.25H_2O$ (**3**), $[(L_{OEt})Gd(TPP)]\cdot 0.25H_2O$ (**4**), $[(L_{OEt})Dy(Pc)]$ (**5**), $[(L_{OEt})Tb(Pc)]$ (**6**), $[(L_{OEt})Ho(Pc)]$ (**7**), and $[(L_{OEt})Gd(Pc)]$ (**8**), where TPP = 5,10,15,20-tetraphenylporphyrinate, and Pc = phthalocyaninate. In the literature, some ytterbium(III), erbium(III), and neodymium(III) complexes of this type were prepared, and their photophysical properties were studied.[10,11] Herein, we focus our studies on both the magnetic properties and the magneto-structural correlation in this unique "4:3 piano stool" seven-coordinate system. Interestingly, the Dy and Tb complexes show field-induced slow relaxation of magnetization, and they are interesting seven-coordinate single-lanthanide-based SMMs.

EXPERIMENTAL SECTION

General Methods. All of the reagents were commercially available and were used without further purification. $Na[(\eta^5\text{-}C_5H_5)Co\{P(=O)(OEt)_2\}_3]$ (NaL_{OEt}) was prepared according to the literature.[12] The syntheses of $[(L_{OEt})Y(Pc)]$ and dilute $[(L_{OEt})Dy(Pc)]$ with $[(L_{OEt})Y(Pc)]$ are presented in the Supporting Information. The elemental analyses for C, H, and N were performed with a Perkin-Elmer 240C analyzer. The melting points were determined with an X-4 digital micro-melting-point apparatus and were uncorrected. The infrared spectra were recorded with a Vector22 Bruker spectrophotometer with KBr pellets in the region from 400 to 4000 cm^{-1}. The UV−vis spectra were obtained with a UV−3600 spectrophotometer in the region from 220 to 1300 nm. The electrospray ionization high-resolution mass spectra (ESI-HRMS) were recorded with a QSTAR mass spectrometer. The magnetic susceptibilities for all polycrystalline samples were measured with a Quantum Design MPMS-SQUID-VSM magnetometer in the temperature range from 1.8 to 300 K. The field dependence of magnetization was measured using a Quantum Design MPMS-SQUID-VSM system in an applied field of up to 70 kOe. The diamagnetic corrections were calculated using Pascal's constants,[13] and an experimental correction for the diamagnetic sample holder was applied.

X-ray Crystallography. The crystal structures were determined with a Siemens (Bruker) SMART CCD diffractometer using monochromated Mo Kα radiation (λ = 0.71073 Å) at 291 K. The cell parameters were retrieved using SMART software and refined using SAINT[14] for all observed reflections. The data was collected using a narrow-frame method with a scan width of 0.30° in ω and an exposure time of 10 s/frame. The highly redundant data sets were reduced using SAINT[14] and corrected both for the Lorentz and polarization effects. The absorption corrections were applied using SADABS[15] supplied by Bruker. The structures were solved by direct methods using the program SHELXL-97.[16] The positions of the metal atoms and their first coordination spheres were located from direct method E-maps. Other nonhydrogen atoms were found in alternating difference Fourier syntheses and least-squares refinement cycles and, during the final cycles, refined anisotropically. Hydrogen atoms were placed in calculated positions and refined as riding atoms with a uniform value of U_{iso}. The final crystallographic data and the values of R1 and wR2 are listed in Table S1 (Supporting Information).

CCDC reference numbers 919 749 (**1**), 919 750 (**2**), 919 751 (**3**), 919 752 (**4**), 919 753 (**5**), 919 754 (**6**), 919 755 (**7**), and 919 756 (**8**).

Synthesis of $[(L_{OEt})Dy(TPP)]\cdot 0.25H_2O$ (1). 5,10,15,20-Tetraphenylporphyrin (24.6 mg, 0.04 mmol), NaL_{OEt} (23.1 mg, 0.04 mmol), and $Dy(acac)_3\cdot 2H_2O$ (18.4 mg, 0.04 mmol) were mixed in 8 mL of $MeCN/CH_3OH$ (1:1 v/v). The resulting mixture was stirred for about 2 h at room temperature, sealed in a 20 mL Teflon-lined stainless steel autoclave, and held at 100 °C for 24 h. The mixture was cooled slowly to room temperature. After the resulting solid was filtered, it was dissolved in 6 mL of $CHCl_3/CH_3OH$ (5:1 v/v) and allowed to stand at room temperature for several days, and purple block-shaped crystals of **1** were obtained. Yield = 25%. Mp > 300 °C. Anal. Calcd for $C_{61}H_{63.5}CoDyN_4O_{9.25}P_3$: C, 55.71; H, 4.87; N, 4.26. Found: C, 55.92; H, 5.05; N, 4.47. ESI-HRMS (positive mode, CH_3OH): m/z = 1311.17 $[M + H]^+$. IR (KBr, cm^{-1}): 3392(w), 2983(m), 1595(m), 1525(m), 1490(m), 1385(m), 1147(s), 1034(s), 810(s), 745(m), 585(m). UV−vis {CH_2Cl_2, λ_{max}/nm, [log (ε/dm^3 mol^{-1} cm^{-1})]}: 223(4.79), 318(4.77), 407(4.89), 426(5.80), 559(4.54), 597(4.04).

Synthesis of $[(L_{OEt})Tb(TPP)]\cdot 0.25H_2O$ (2). The purple block-shaped crystals of complex **2** were obtained by following the same procedure as that described for complex **1** except that $Tb(acac)_3\cdot 2H_2O$ was used instead of $Dy(acac)_3\cdot 2H_2O$. Yield = 18%. Mp > 300 °C. Anal. Calcd for $C_{61}H_{63.5}CoTbN_4O_{9.25}P_3$: C, 55.87; H, 4.88; N, 4.27. Found: C, 56.09; H, 5.11; N, 4.56. ESI-HRMS (positive mode, CH_3OH): m/z = 1307.17 $[M + H]^+$. IR (KBr, cm^{-1}): 3398(w), 2977(m), 1635(m), 1602(m), 1474(m), 1384(m), 1135(s), 1037(s), 816(m), 735(m), 582(m). UV−vis {CH_2Cl_2, λ_{max}/nm, [log (ε/dm^3 mol^{-1} cm^{-1})]}: 221(4.81), 319(4.46), 407(4.89), 426(5.80), 559(4.53), 598(4.03).

Synthesis of $[(L_{OEt})Ho(TPP)]\cdot 0.25H_2O$ (3). The purple block-shaped crystals of complex **3** were obtained by following the same procedure as that described for complex **1** except that $Ho(acac)_3\cdot 2H_2O$ was used instead of $Dy(acac)_3\cdot 2H_2O$. Yield = 22%. Mp > 300 °C. Anal. Calcd for $C_{61}H_{63.5}CoHoN_4O_{9.25}P_3$: C, 55.61; H, 4.86; N, 4.25. Found: C, 55.81; H, 5.09; N, 4.43. ESI-HRMS (positive mode, CH_3OH): m/z = 1313.25 $[M + H]^+$. IR (KBr, cm^{-1}): 3396(w), 2973(m), 2360(m), 1593(m), 1474(m), 1395(m), 1133(s), 1041(s), 836(m), 749(m), 580(m). UV−vis {CH_2Cl_2, λ_{max}/nm, [log (ε/dm^3 mol^{-1} cm^{-1})]}: 221(4.80), 319(4.50), 406(4.92), 427(5.79), 559(4.58), 598(4.05).

Synthesis of $[(L_{OEt})Gd(TPP)]\cdot 0.25H_2O$ (4). The purple block-shaped crystals of complex **4** were obtained by following the same procedure as that described for complex **1** except that $Gd(acac)_3\cdot 2H_2O$ was used instead of $Dy(acac)_3\cdot 2H_2O$. Yield = 19%. Mp > 300 °C. Anal. Calcd for $C_{61}H_{63.5}CoGdN_4O_{9.25}P_3$: C, 55.94; H, 4.89; N, 4.28. Found: C, 56.11; H, 5.15; N, 4.58. ESI-HRMS (positive

dx.doi.org/10.1021/ic400245n | Inorg. Chem. 2013, 52, 6407−6416

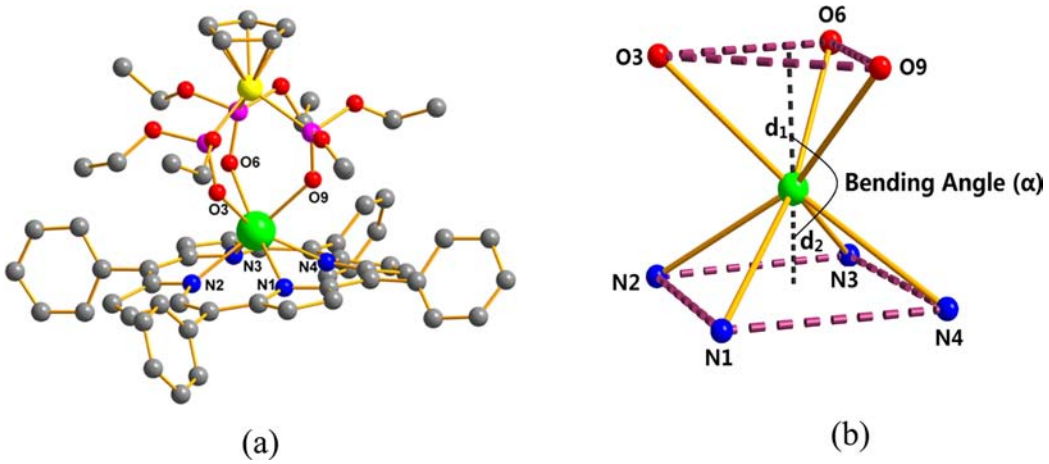

Figure 1. (a) Crystal structure of complexes **1**−**4**. Hydrogen atoms and solvent molecules are omitted for clarity. Ln, green (Ln = Dy for **1**, Tb for **2**, Ho for **3**, Gd for **4**); Co, yellow; N, blue; P, purple; O, red; and C, gray. (b) Local coordination geometry of Ln(III) ion (Ln = Dy for **1**, Tb for **2**, Ho for **3**, Gd for **4**). d_1 and d_2 represent the distance from Ln to either the center of the O_3 plane (O3, O6, O9) or the N_4 plane (N1, N2, N3, N4), respectively. α is the bending angle of center−Ln−center.

mode, CH_3OH): m/z = 1306.17 $[M + H]^+$. IR (KBr, cm^{-1}): 3395(w), 2975(m), 1637(m), 1598(m), 1491(m), 1383(m), 1125(s), 1050(s), 832(m), 735(m), 590(m). UV−vis {CH_2Cl_2, λ_{max}/nm, [log (ε/dm^3 mol^{-1} cm^{-1})]}: 222(4.69), 319(4.47), 407(4.89), 426(5.78), 559(4.54), 598(4.07).

Synthesis of [(L_{OEt})Dy(Pc)] (5). Phthalocyanine (20.6 mg, 0.04 mmol), NaL_{OEt} (23.1 mg, 0.04 mmol), and $Dy(acac)_3{\cdot}2H_2O$ (18.4 mg, 0.04 mmol) were mixed in 8 mL of MeCN/CH_3OH (1:1 v/v). The resulting mixture was stirred for about 2 h at room temperature, sealed in a 20 mL Teflon-lined stainless steel autoclave, and held at 100 °C for 24 h. The mixture was cooled slowly to room temperature. After the resulting solid was filtered, it was dissolved in 6 mL of $CHCl_3$/CH_3OH (5:1 v/v) and allowed to stand at room temperature for several days, and blue block-shaped crystals of **5** were obtained. Yield = 30%. Mp > 300 °C. Anal. Calcd for $C_{49}H_{51}CoDyN_8O_9P_3$: C, 48.63; H, 4.25; N, 9.26. Found: C, 48.89; H, 4.39; N, 9.53. ESI-HRMS (positive mode, CH_3OH): m/z = 1212.08 $[M + H]^+$. IR (KBr, cm^{-1}): 3389(m), 2973(m), 1605(m), 1480(s), 1401(m), 1328(s), 1159(s), 1050(m), 927(s), 839(m), 725(m), 586(s). UV−vis {CH_2Cl_2, λ_{max}/nm, [log (ε/dm^3 mol^{-1} cm^{-1})]}: 243(5.01), 343(5.00), 606(4.74), 642(4.70), 671(5.56).

Synthesis of [(L_{OEt})Tb(Pc)] (6). The blue block-shaped crystals of complex **6** were obtained by following the same procedure as that described for complex **5** except that $Tb(acac)_3{\cdot}2H_2O$ was used instead of $Dy(acac)_3{\cdot}2H_2O$. Yield = 28%. Mp > 300 °C. Anal. Calcd for $C_{49}H_{51}CoTbN_8O_9P_3$: C, 48.77; H, 4.26; N, 9.29. Found: C, 48.99; H, 4.55; N, 9.51. ESI-HRMS (positive mode, CH_3OH): m/z = 1207.25 $[M + H]^+$. IR (KBr, cm^{-1}): 3400(m), 2973(m), 1608(m), 1479(s), 1451(m), 1328(s), 1159(s), 1058(m), 929(s), 839(m), 729(m), 588(s). UV−vis {CH_2Cl_2, λ_{max}/nm, [log (ε/dm^3 mol^{-1} cm^{-1})]}: 244(5.05), 344(5.04), 606(4.78), 643(4.73), 671(5.59).

Synthesis of [(L_{OEt})Ho(Pc)] (7). The blue block-shaped crystals of complex **7** were obtained by following the same procedure as described for complex **5** except that $Ho(acac)_3{\cdot}2H_2O$ was used instead of $Dy(acac)_3{\cdot}2H_2O$. Yield = 28%. Mp > 300 °C. Anal. Calcd for $C_{49}H_{51}CoHoN_8O_9P_3$: C, 48.53; H, 4.24; N, 9.24. Found: C, 48.74; H, 4.50; N, 9.49. ESI-HRMS (positive mode, CH_3OH): m/z = 1213.25 $[M + H]^+$. IR (KBr, cm^{-1}): 3416(m), 2973(m), 1606(m), 1480(s), 1453(m), 1328(s), 1159(s), 1059(m), 929(s), 839(m), 730(m), 588(s). UV−vis {CH_2Cl_2, λ_{max}/nm, [log (ε/dm^3 mol^{-1} cm^{-1})]}: 243(5.07), 344(5.06), 606(4.81), 642(4.76), 671(5.62).

Synthesis of [(L_{OEt})Gd(Pc)] (8). The blue block-shaped crystals of complex **8** were obtained by following the same procedure as that described for complex **5** except that $Gd(acac)_3{\cdot}2H_2O$ was used instead of $Dy(acac)_3{\cdot}2H_2O$. Yield = 23%. Mp > 300 °C. Anal. Calcd for $C_{49}H_{51}CoGdN_8O_9P_3$: C, 48.84; H, 4.27; N, 9.30. Found: C, 49.03; H, 4.44; N, 9.58. ESI-HRMS (positive mode, CH_3OH): m/z = 1206.25 $[M + H]^+$. IR (KBr, cm^{-1}): 3410(m), 2973(m), 1606(m), 1478(s), 1451(m), 1328(s), 1159(s), 1080(m), 928(s), 839(m), 728(s), 587(s). UV−vis {CH_2Cl_2, λ_{max}/nm, [log (ε/dm^3 mol^{-1} cm^{-1})]}: 243(5.04), 344(5.01), 606(4.73), 642(4.70), 671(5.53).

RESULTS AND DISCUSSION

All of the complexes were successfully and efficiently isolated by the reaction of equimolar amounts of the tripodal ligand L_{OEt}^-, the porphyrinate (or phthalocyaninate) ligand, and lanthanide acetylacetonates. Suitable single crystals for X-ray diffraction analysis were obtained by the slow evaporation of the solution of these complexes in methanol and chloroform. The electronic absorption spectra of the porphyrinate or phthalocyaninate complexes in solution are almost identical (Figures S1 and S2, Supporting Information). For complexes **1**−**4**, the absorption bands at around 426, 559, and 597 nm can be assigned to the intraligand $\pi-\pi^*$ transitions of the porphyrinate ligand, whereas complexes **5**−**8** also show typical feature of phthalocyaninate metal complexes with a strong Q band at 671 nm and two additional weak bands at around 606 and 643 nm.[10,11]

Structural Description. Complexes **1**−**4** crystallize in the *C*2/*c* space group, and their structures are similar to those previously reported in the literature.[11] Selected bond lengths and bond angles are given in Table S2 (Supporting Information). The lanthanide(III) ions (Ln = Dy for **1**, Tb for **2**, Ho for **3**, Gd for **4**) are seven-coordinate and are surrounded by four N atoms of the porphyrinate dianion and three O atoms from the anionic tripodal ligand L_{OEt}^- (Figure 1a). The coordination geometry of the Ln(III) ions can be described as a 4:3 piano stool,[17] with three O atoms of the tripodal ligand forming the triangular plane and the porphyrin occupying the square base (Figure 1b). The Ln−N bond length ranges from 2.396(4) to 2.407(4) Å for **1**, 2.396(4) to 2.409(5) Å for **2**, 2.393(5) to 2.410(5) Å for **3**, and 2.393(4) to 2.417(5) Å for **4**, whereas the Ln−O bond length ranges from 2.298(4) to 2.339(4) Å for **1**, 2.294(4) to 2.330(4) Å for **2**, 2.306(4) to 2.332(4) Å for **3**, and 2.292(4) to 2.336(4) Å for **4**. The distances of the Ln^{3+} ions from the porphyrin plane (N1, N2, N3, N4) center are 1.218 Å for **1**, 1.229 Å for **2**, 1.223 Å for **3**, and 1.233 Å for **4**, which are closer than those of the triangular

dx.doi.org/10.1021/ic400245n | Inorg. Chem. 2013, 52, 6407−6416

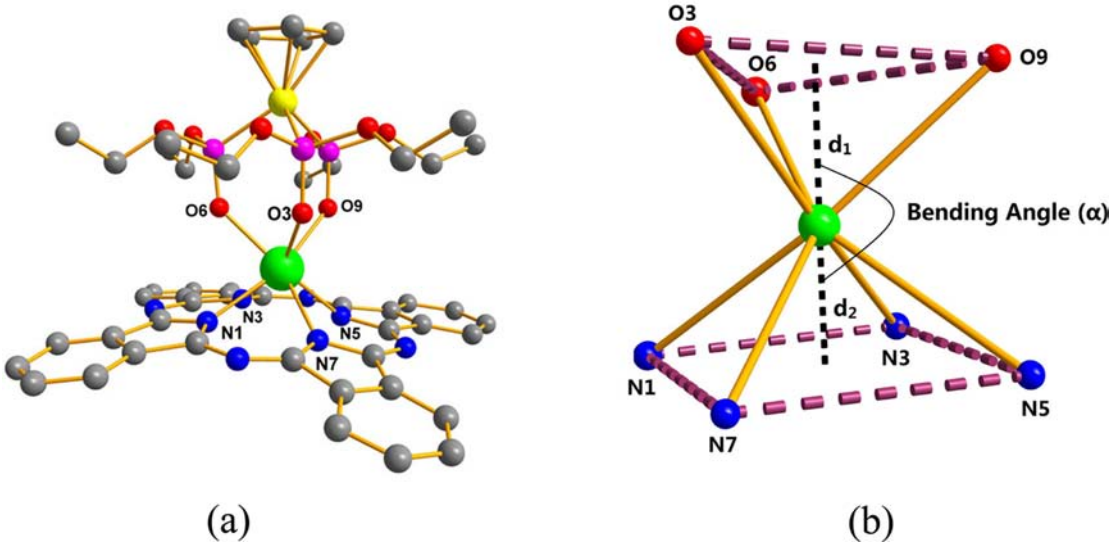

Figure 2. (a) Crystal structure of complexes **5**–**8**. Hydrogen atoms are omitted for clarity. Ln, green (Ln = Dy for **5**, Tb for **6**, Ho for **7**, Gd for **8**); Co, yellow; N, blue; P, purple; O, red; and C, gray. (b) Local coordination geometry of Ln(III) ion (Ln = Dy for **5**, Tb for **6**, Ho for **7**, Gd for **8**).

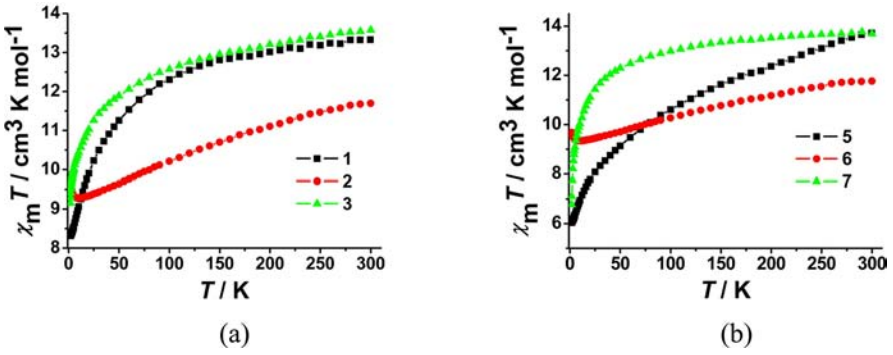

Figure 3. (a) Temperature dependence of the $\chi_M T$ values for complexes **1**–**3** with an applied field of 100 Oe. (b) Temperature dependence of the $\chi_M T$ values for complexes **5**–**7** with an applied field of 100 Oe.

plane (O3, O6, O9) center (1.585 Å for **1**, 1.587 Å for **2**, 1.584 Å for **3**, and 1.592 Å for **4**). Furthermore, the tripodal ligand O_3 plane and the porphyrin N_4 plane are almost parallel to one another with a dihedral angle of 2.83° for **1**, 2.93° for **2**, 2.87° for **3**, and 2.73° for **4**, and the bending angles, defined as the center–Ln–center, are 176.57° for **1**, 176.42° for **2**, 176.65° for **3**, and 176.34° for **4**. There is no significant intermolecular interaction (as shown in Figure S3 for the packing diagram, Supporting Information). The shortest intermolecular Ln^{3+}–Ln^{3+} distance is 10.097 Å for **1**, 10.114 Å for **2**, 10.088 Å for **3**, and 10.135 Å for **4**.

Complexes **5**–**8** also show similar double-decker sandwich crystal structures to those of **1**–**4**. Selected bond lengths and bond angles are given in Table S3 (Supporting Information). As shown in Figure 2a, the lanthanide(III) ions (Ln = Dy for **5**, Tb for **6**, Ho for **7**, Gd for **8**) are seven-coordinate, and the coordination geometry of the Ln(III) ions can also be described as a 4:3 piano stool, with the triangular plane from three O atoms of the tripodal ligand and the square base from four N atoms of the phthalocyaninate ligand (Figure 2b). The average Ln–N distances (2.378 Å for **5**, 2.391 Å for **6**, 2.372 Å for **7**, and 2.378 Å for **8**) are also longer than the average Ln–O distances (2.257 Å for **5**, 2.271 Å for **6**, 2.252 Å for **7**, and 2.261 Å for **8**), reflecting the higher affinity of the Ln^{3+} ions for the O atoms over the N atoms. The distance from the Ln^{3+} ion to the mean plane center of the O_3 plane and the N_4 plane is 1.503 and 1.317 Å for **5**, 1.522 and 1.338 Å for **6**, 1.496 and 1.295 Å for **7**, and 1.510 and 1.312 Å for **8**, respectively. The dihedral angles between the triangular and square planes are 7.20° for **5**, 7.48° for **6**, 7.13° for **7**, and 7.34° for **8**, whereas the bending angles are 173.64° for **5**, 173.88° for **6**, 174.20° for **7**, and 174.15° for **8**. The packing diagram is shown in Figure S4 (Supporting Information). The shortest intermolecular distance between Ln^{3+}–Ln^{3+} ions is 9.918 Å for **5**, 9.908 Å for **6**, 9.897 Å for **7**, and 9.973 Å for **8**.

Static Magnetic Properties. The direct current (dc) magnetic measurements were performed on polycrystalline samples for all of the complexes in the range of 1.8 to 300 K under an external field of 100 Oe. No detailed discussions on complexes **4** and **8** with Gd(III) ion are made because they are within the normal values of $S = {}^7/_2$ (half-filled f orbital) for a mononuclear complex. At 300 K, the $\chi_M T$ values are 13.33, 11.70, and 13.57 cm^3 K mol^{-1} for **1**, **2**, and **3**, respectively. They are slightly smaller than the expected paramagnetic values of 14.17, 11.82, and 14.07 cm^3 K mol^{-1} for Dy(III) ($^6H_{15/2}$, $S = {}^5/_2$, $L = 5$, $J = {}^{15}/_2$, $g = {}^4/_3$), Tb(III) ($^7F_6$, $S = 3$, $L = 3$, $J = 6$, $g = {}^3/_2$), and Ho(III) ($^5I_8$, $S = 2$, $L = 6$, $J = 8$, $g = {}^5/_4$) (Figure 3a). At the same temperature, the observed $\chi_M T$ values are 13.72, 11.77, and 13.68 cm^3 K mol^{-1} for **5**, **6**, and **7**, respectively. They are close to those of **1**–**3** (Figure 3b). On cooling, each $\chi_M T$

dx.doi.org/10.1021/ic400245n | Inorg. Chem. 2013, 52, 6407–6416

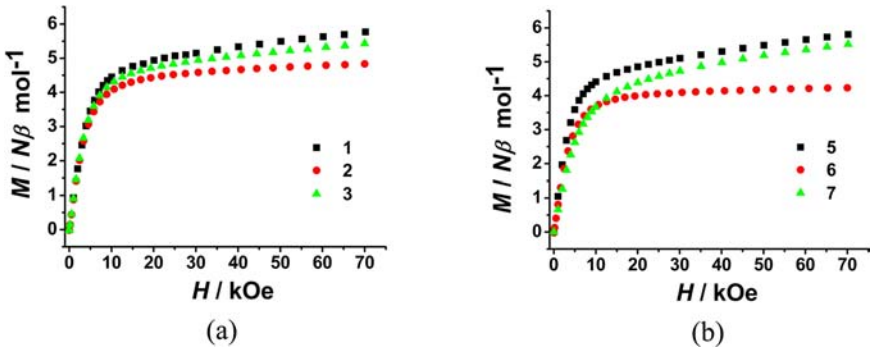

Figure 4. (a) Plots of magnetization upon the application of a magnetic field from 0 to 7 T at 1.8 K for complexes **1**−**3**. (b) Plots of magnetization upon the application of a magnetic field from 0 to 7 T at 1.8 K for complexes **5**−**7**.

value gradually decreases from 300 to 1.8 K, which may be ascribed to the progressive depopulation of the Stark level split by the ligand field.[18,19] In contrast, the $\chi_M T$ values slowly reach a corresponding minimum of 9.28 cm^3 K mol^{-1} for **2** at 12.0 K and 9.34 cm^3 K mol^{-1} for **6** at 14.0 K and then slightly increase to 9.61 and 9.68 cm^3 K mol^{-1} at 1.8 K, respectively. The unusual small upturn observed at the low temperature may be due to the weak intermolecular dipolar interations.[20]

The magnetizations of complexes **1**−**3** and **5**−**7** from a zero dc field to 70 kOe at 1.8 K are shown in Figure 4a,b. For **1**−**3**, the magnetization increases rapidly at low field and then slowly reaches values of 5.76, 4.83, and 5.42 Nβ at 70 kOe for **1**, **2**, and **3**, respectively. They are lower than the theoretical values of 10 Nβ for Dy and Ho and 9 Nβ for Tb. In contrast, the magnetization reaches values of 5.80 Nβ for **5**, 4.23 Nβ for **6**, and 5.51 Nβ for **7** at 70 kOe, which also deviates from the theoretical saturation values. These maximum values are smaller than the expected saturation values and can be attributed to the ligand-field-induced splitting of the Stark level as well as magnetic anisotropy with a lower effective spin.[21]

Dynamic Magnetic Properties. The investigation of the slow magnetization of relaxation was carried out via alternating current (ac) susceptibility measurements. At zero external field, no out-of-phase signal (χ'') for the ac susceptibilities are observed at frequencies of up to 999 Hz and at temperatures down to 1.8 K for all of the complexes. Under an intermediate dc field (2 kOe), only **1**, **2**, **5**, and **6** show obvious χ'' susceptibility signals above 1.8 K, suggesting the presence of an activated relaxation process. However, Ho and Gd complexes in both porphyrin and phthalocyanine systems do not show observable χ'' signals under a 2 kOe dc field. The reason is that Gd(III) has half-filled f^7 shells with a ground state configuration that is expected to be isotropic, whereas Ho complexes **3** and **7** belong to a non-Kramers' system with even numbers of 4f electrons and have a nondegenerate ground state with large energy gaps between the ground state and the lowest excited state. Compared to the Ho and Gd complexes, the Dy and Tb complexes lie in the larger and specific anisotropy of single Dy(III) and Tb(III) ions (Kramers' and non-Kramers', respectively), leading to a large effect of ligand-field potential on the magnetization of relaxation-quenching quantum tunneling of the magnetization (QTM) through the spin-reversal barrier upon application of a static field.[8,22] The energy barrier (Δ/k_B), based on the Arrhenius law, for complexes **1**, **2**, **5**, and **6** is summarized in Table 1.

*Dynamic Magnetic Properties of Dy Complexes **1** and **5**.* For complex **1**, the temperature dependence of both the in-phase (χ') and out-of-phase (χ'') signals is observed at a static field of 2 kOe (Figure 5a). Below 3.5 K, the peaks of the χ'' signal can be found at frequencies higher than 400 Hz, and the relaxation followed a thermally activated mechanism affording an energy barrier (Δ/k_B) of 8.5 K, with a pre-exponential factor τ_0 of 6.3×10^{-6} s based on the Arrhenius law [$\tau = \tau_0 \exp(\Delta/k_BT)$] ($R = 0.9953$) (Figure 5b), where T is the temperature of the maximum χ'' at different frequencies and $\tau = 1/(2\pi\upsilon)$ (υ is the frequency).[23−25] The Cole−Cole plots on the basis of frequency-dependent ac susceptibilities are illustrated in Figures S5 and S6 (Supporting Information) for the observation of the magnetic relaxation process. They show a well-shaped arc, suggesting a distribution of single relaxation processes that is due to one kind of coordination environment around the lanthanide ion in the molecule. The irregularity at low temperatures can be ascribed to the stronger quantum tunneling effects.[26−28]

Table 1. Summary of the Average Ln−N and Ln−O Bond Distances, Ln-to-Plane Center Distances, Plane Center Distances, Dihedral Angles between Different Planes, Bending Angles, and the Energy Barrier for Complexes 1, 2, 5, and 6

	1 (Dy)	2 (Tb)	5 (Dy)	6 (Tb)
average Ln−N bond distance (Å)	2.402	2.403	2.378	2.391
average Ln−O bond distance (Å)	2.314	2.312	2.257	2.271
Ln to O_3 plane center distance (d_1, Å)	1.585	1.587	1.503	1.522
Ln to N_4 plane center distance (d_2, Å)	1.218	1.229	1.317	1.338
distance between O_3−N_4 plane centers (l, Å)	2.802	2.814	2.816	2.856
dihedral angle between O_3−N_4 planes (ϕ, deg)	2.83	2.93	7.20	7.48
bending angle (α, deg)	176.57	176.42	173.64	173.88
$\Delta d^a = \lvert d_1 - d_2 \rvert$ (Å)	0.367	0.358	0.186	0.184
$\Delta/k_B{}^b$ (K)	8.5	16.4	23.6	19.0

[a]The difference in the distance between the Ln^{3+} ion to two plane centers. [b]Energy barrier based on the Arrhenius law [$\tau = \tau_0 \exp(\Delta/k_BT)$].

For complex **5**, the maximum peaks of the χ'' signal can be found above 64 Hz in the temperature range of 2.0 to 4.0 K (Figure 6a). The Arrhenius law fit of the magnetization−relaxation parameter based on temperature-dependent ac susceptibilities afford an energy barrier of 23.6 K with a relaxation time of 1.4×10^{-7} s ($R = 0.9965$) (Figure 6b).

The frequency-dependent ac susceptibilities were measured under a 2 kOe dc field for **5** in the temperature range of 2.0 to

dx.doi.org/10.1021/ic400245n | Inorg. Chem. 2013, 52, 6407−6416

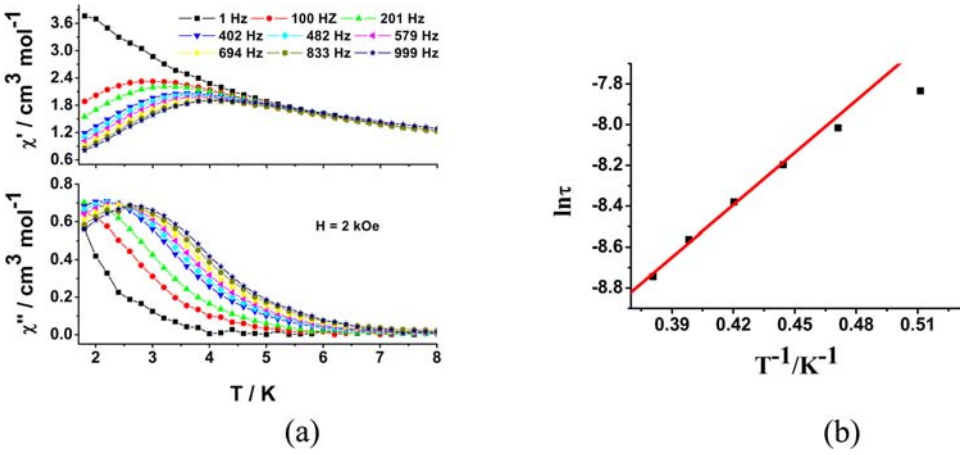

Figure 5. (a) Temperature dependence of the in-phase (χ') and out-of-phase (χ'') signals at different frequencies for **1** at 2 kOe. (b) Arrhenius fit of the ln τ vs T^{-1} plot for **1**. The red solid line represents the best fit of the data.

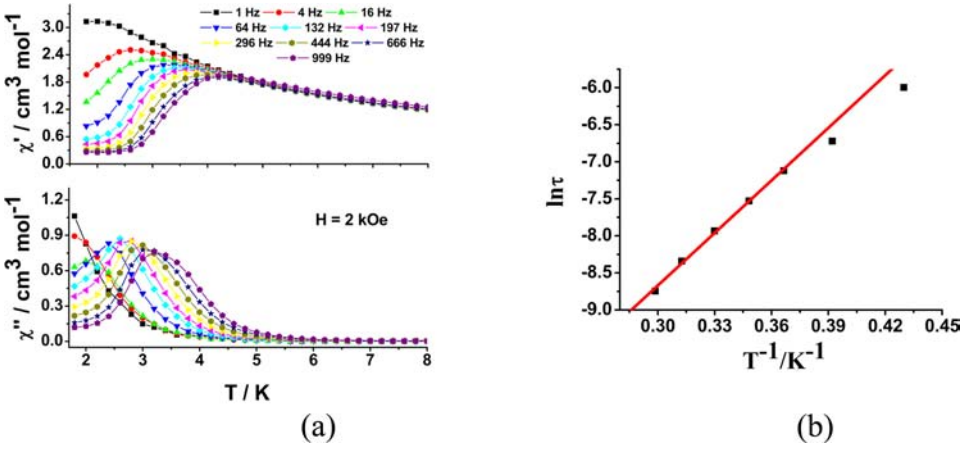

Figure 6. (a) Temperature dependence of the in-phase (χ') and out-of-phase (χ'') signals at different frequencies for **5** at 2 kOe. (b) Arrhenius fit of the ln τ vs T^{-1} plot for **5**. The red solid line represents the best fit of the data.

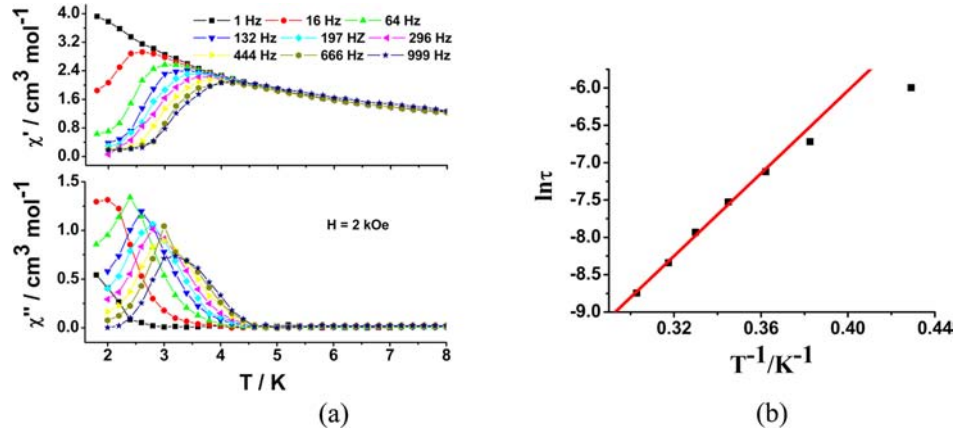

Figure 7. (a) Temperature dependence of the in-phase (χ') and out-of-phase (χ'') signals at different frequencies for the diluted complex **5**, L_{OEt}-Dy(Y)-Pc, at 2 kOe. (b) Arrhenius fit of the ln τ vs T^{-1} plot for the diluted complex **5**. The red solid line represents the best fit of the data.

3.5 K (Figure S7, Supporting Information). The maximum peak of χ'' exhibits a gradual shift toward the low-frequency region as the temperature is decreased. Similar to that of complex **1**, this irregularity is also observed in the Cole−Cole plots (Figure S8, Supporting Information), and the attempt to fit the data by the modified Debye model[26] is unreasonable because of the stronger quantum tunneling effects at lower temperatures.

The dynamic magnetic behaviors for SMMs containing single rare-earth metal ions are closely related to the differences between the coordination environments of the central metal ions. As summarized in Table 1, the following parameters are used to evaluate the effect of a lowered symmetrical ligand field on the anisotropy of lanthanide ions in single-ion molecular magnets: metal-to-plane distances (d_1, d_2, Δd), plane center

dx.doi.org/10.1021/ic400245n | Inorg. Chem. 2013, 52, 6407−6416

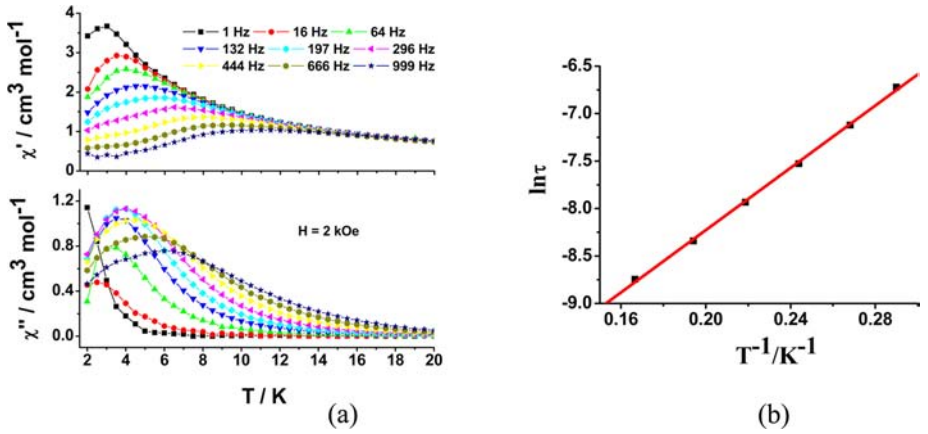

Figure 8. (a) Temperature dependence of the in-phase (χ') and out-of-phase (χ'') signals at different frequencies for **2** at 2 kOe. (b) Arrhenius fit of the ln τ vs T^{-1} plot for **2**. The red solid line represents the best fit of the data.

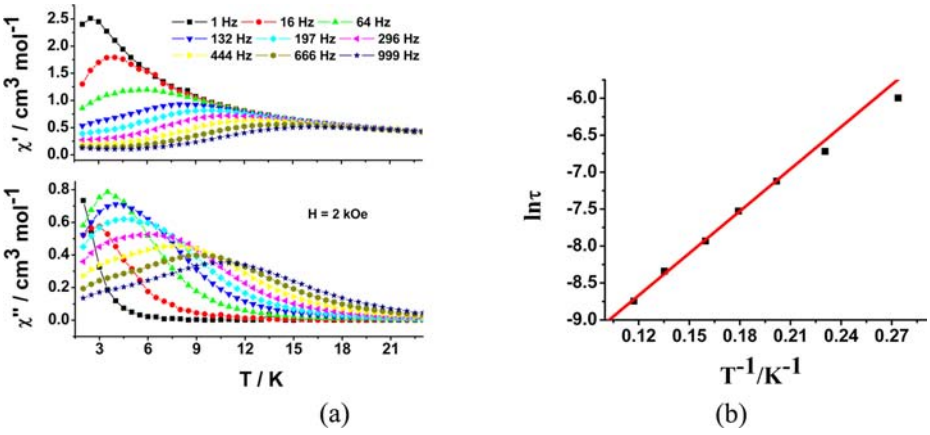

Figure 9. (a) Temperature dependence of the in-phase (χ') and out-of-phase (χ'') signals at different frequencies for **6** at 2 kOe. (b) Arrhenius fit of the ln τ vs T^{-1} plot for **6**. The red solid line represents the best fit of the data.

distances (l), dihedral angles between different planes (ϕ), and bending angles (α). For **1**, the distances between Dy^{3+} to the two plane centers are 1.585 and 1.218 Å, giving a distance difference (Δd) of 0.367 Å, whereas the related Δd value is 0.186 Å for complex **5**. Thus, the effect of the ligand field on the lanthanide ions is different between **1** and **5**. Additionally, the bending angle is 176.57° for **1**, which is larger than that for **5** (173.64°), and the distance between the tripodal ligand O_3 plane center and the porphyrin N_4 plane center is shorter than that of the O_3 plane center and the phthalocyanine N_4 plane center. Indeed, the slow magnetic relaxation is affected by the local molecular symmetry and is sensitive to subtle distortions of the coordination geometry of the 4f ions.[29] The energy barrier for **1** (8.5 K) is lower than that for **5** (23.6 K). Compared to a similar seven-coordinate mononuclear Dy complex with a salen-type ligand (Dy-salen),[9] the energy barrier for complex **5** is obviously increased (13.3 K for Dy-salen), suggesting that the rigid macrocyclic phthalocyaninate ligand generates higher local symmetry than the salen-type ligand, whereas the reversal energy barriers of **1** and **5** are lower in comparison to the eight-coordinate mononuclear double-decker $[DyPc_2]^-$. The η^3-tripodal ligand (L_{OEt}^-) in our sandwich-type system is the weaker ligand compared to Pc^{2-}, and the magnetic relaxation process may be influenced by the weakened strength of the ligand field because of the decreased coordination number and crystal field symmetry.

To reduce the dipole−dipole interaction between magnetic centers, magnetic measurements on samples in which complex **5** was diluted by the isostructural Y^{3+} analogue in a molar ratio of 1:10 (Supporting Information) were performed. For the diluted samples, the temperature dependence of the ac magnetic susceptibilities at H_{dc} = 0 (Figure S9, Supporting Information) and at 2 kOe (Figure 7a) was recorded. Under a zero dc field, weak peaks can be observed in χ'' with a maximum located at around 3.0 K above 111 Hz. However, the susceptibilities still increase with decreasing temperature, which suggests that quantum tunneling acts on the relaxation process in the low-temperature region.[20,30] When a field of 2 kOe is applied, the quantum tunneling of the magnetization is suppressed and the peaks of the χ'' signal can be observed at frequencies as low as 64 Hz. The energy barrier obtained by modeling the behavior with the Arrhenius law is 27.7 K, with a relaxation time of 3.7×10^{-8} s (R = 0.9959) (Figure 7b).

The Cole−Cole plots, based on the frequency-dependent ac susceptibilities from 2.0 to 3.5 K, show semicircular shapes, and the data are fitted to a generalized Debye[31] model, leading to values of α in the range of 0.11 to 0.23 (Figures S10 and S11, Supporting Information). Remarkably, the magnetic dynamic studies of complex **5** diluted in diamagnetic Y analogue indicate that the dipole−dipole interaction between the Dy^{3+} sites is remarkably weakened and that the quantum tunneling effects are suppressed at lower temperatures.[32]

dx.doi.org/10.1021/ic400245n | Inorg. Chem. 2013, 52, 6407−6416

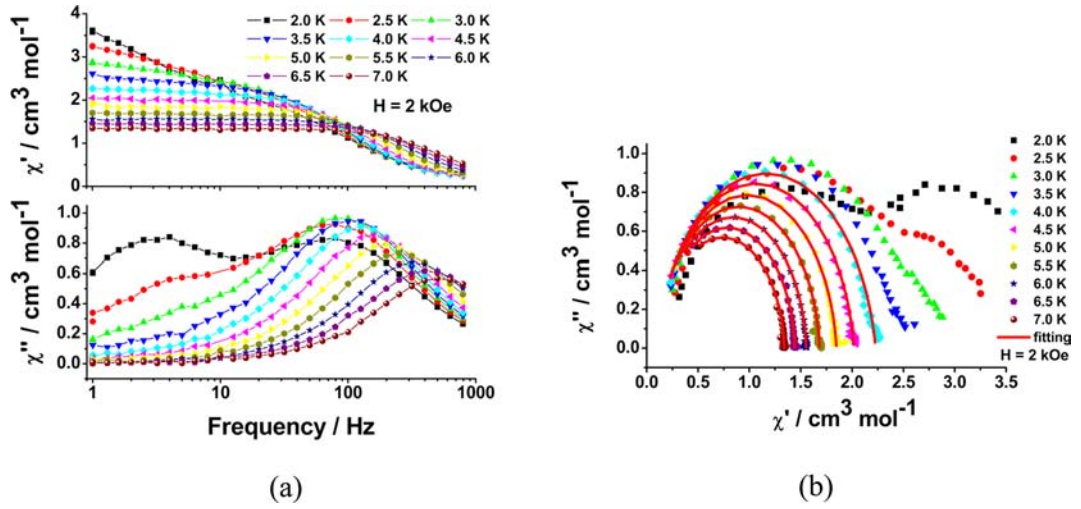

Figure 10. (a) Frequency dependence of the in-phase (χ') and out-of-phase (χ'') signals for **2** from 2.0 to 7.0 K at a 2 kOe dc field. The solid lines are only guides. (b) Cole−Cole plots for **2** obtained using the ac susceptibility data at a 2 kOe dc field. The red solid lines correspond to the fit obtained to a general Debye model from 4.0 to 7.0 K. In the plots, α = 0.10, 0.07, 0.06, 0.05, 0.04, 0.03, and 0.03 at 4.0, 4.5, 5.0, 5.5, 6.0, 6.5, and 7.0 K, respectively.

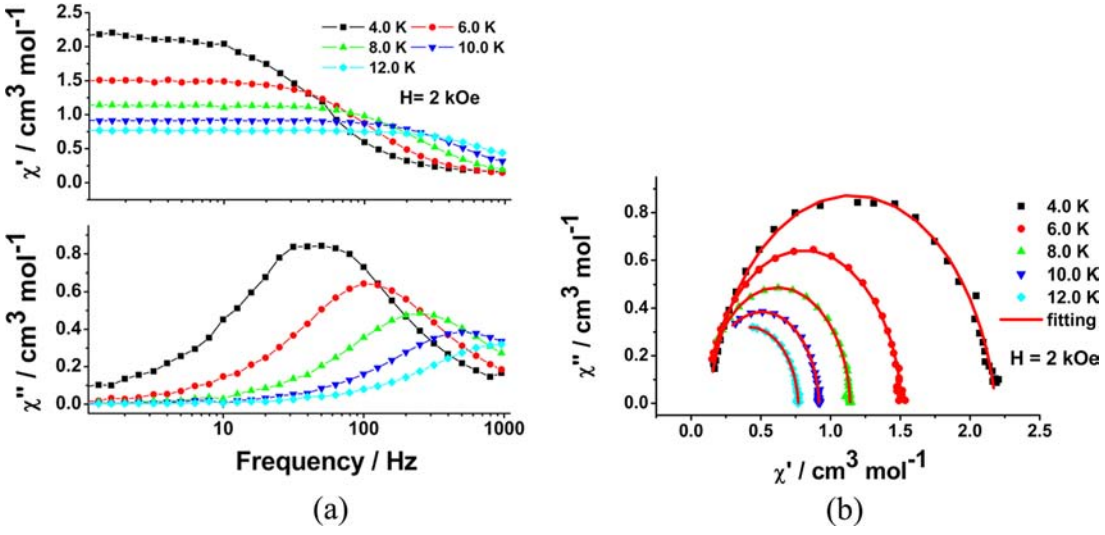

Figure 11. (a) Frequency dependence of the in-phase (χ') and out-of-phase (χ'') signals for **6** from 4.0 to 12.0 K at a 2 kOe dc field. The solid lines are only guides. (b) Cole−Cole plots for **6** obtained using the ac susceptibility data at a 2 kOe dc field. The red solid lines correspond to the fit obtained to a general Debye model. In the plots, α = 0.10, 0.05, 0.04, 0.03, and 0.05 at 4.0, 6.0, 8.0, 10.0, and 12.0 K, respectively.

*Dynamic Magnetic Properties of Tb Complexes **2** and **6**.* The clear χ'' signals for **2** can be found at frequencies higher than 64 Hz in the temperature range of 3.0 to 8.0 K (Figure 8a), whereas the maximum peak of the χ'' signal for **6** is observed in the temperature range of 3.0 to 12.0 K (Figure 9a). A corresponding Arrhenius law fit of the data gives an energy barrier of 16.4 K and a relaxation time of 1.0×10^{-5} s for **2** (R = 0.9987) (Figure 8b) and an energy barrier of 19.0 K and a relaxation time of 1.7×10^{-5} s for **6** (R = 0.9979) (Figure 9b).

The frequency-dependent ac susceptibilities were also measured for **2** and **6** with various ac frequencies at H_{dc} = 2 kOe (Figures 10a and 11a). For complex **2**, the Cole−Cole plots show semicircular shapes for temperatures higher than 4.0 K (Figure 10b). The data can be fit to a generalized Debye model, and the α parameter is in the range from 0.03 to 0.10 (α = 0 for an ideal Debye model with a single relaxation time). When the system enters the quantum regime (below 4.0 K), a slight asymmetry in the Cole−Cole plots appears, which indicates a narrow width of the distribution in this single relaxation process.[27,33]

The semicircular shapes of the Cole−Cole plots for **6** are also observed from 4.0 to 12.0 K (Figure 11b), and the α parameter, fit to a generalized Debye model, is in the range of 0.03 to 0.10, also indicating that the relaxation followed a thermally activated mechanism above 4.0 K with only a single magnetic relaxation process.

The ligand-field effect is a key factor in the slowly relaxing magnetic behavior in lanthanide-based complexes, which is confirmed by the differences in slow relaxation observed for **1** (with porphyrin) and **5** (with phthalocyanine). However, the difference between **2** and **6** is not so obvious, which may be attributed to the nature of the Dy and Tb ions. Complexes **1** and **2** are isomorphous, as are complexes **5** and **6**. The structural difference between **1** and **5** is almost the same as that between **2** and **6** (Table 1). In our previous work, the magnetic relaxation dynamics of a mononuclear Tb complex with a salen-

dx.doi.org/10.1021/ic400245n | Inorg. Chem. 2013, 52, 6407−6416

type ligand (Tb-salen) were not observed, even under an intermediate dc field (2 kOe).[9] In contrast, both Tb complexes in the porphyrin and the phthalocyanine systems show field-induced slow magnetic relaxation at a higher temperature range, mainly resulting from the characteristic ligand-field splitting pattern of the $J = 6$ ground multiplet of the Tb(III) ion with a $4f^8$ electronic configuration. This is consistent with that of other Tb−Pc sandwich complexes.[6,34−36] The lower reversal energy barriers and blocking temperatures for **2** and **6** when compared to those for $[TbPc_2]^-$ may also be related to the strength of the ligand field. Additionally, the three donor O atoms of the tripodal ligand do not match the extending direction of f electron orbitals, such as $f_{z(x^2-y^2)}$ and f_{xyz}. Therefore, the effect of the ligand field that leads to a strengthening of the anisotropy of the Tb(III) ion is smaller in **2** and **6** than that of $[TbPc_2]^-$. Further structural and magnetic information about more complexes of this type is necessary for us to understand the correlation between magnetic properties and the crystal field coordination environment.

CONCLUSIONS

A series of new seven-coordinate paramagnetic lanthanide complexes based the Kläui's tripodal ligand and the porphyrin (or phthalocyanine) ligand have been successfully synthesized. All of the complexes are characterized by X-ray crystallography and show similar double-decker sandwich structures. Magnetic measurements revealed that the Dy and Tb complexes exhibit a field-induced slow relaxation of magnetization and are seven-coordinate single lanthanide-based SMMs. The effect of doping on the magnetic relaxation of the L_{OEt}-Dy(Y)-Pc complex indicates that the dipole−dipole interaction and quantum tunneling effects are remarkably suppressed. The results confirm that the magnetic relaxation properties of these double-decker sandwich complexes are affected by the local molecular symmetry and are very sensitive to tiny distortions in the coordination geometry of the paramagnetic lanthanide ions. In future work, we aim to synthesize more complexes of this type and to tune the dynamics of magnetization in single-lanthanide-based SMMs by controlling the single-ion anisotropy and/or the crystal field environment.

ASSOCIATED CONTENT

Supporting Information

Additional experimental details, structures and magnetic characterization data, and X-ray crystallographic files in CIF format for **1**−**8**. This material is available free of charge via the Internet at http://pubs.acs.org.

AUTHOR INFORMATION

Corresponding Author

*E-mail: zuojl@nju.edu.cn (J.-L.Z.); yousong@nju.edu.cn (Y.S.). Fax: +86 25 83314502.

Notes

The authors declare no competing financial interest.

ACKNOWLEDGMENTS

This work was supported by the Major State Basic Research Development Program (2011CB808704 and 2013CB922100) and the National Natural Science Foundation of China (21171089, 21021062 and 91022031). We also thank Dr. Tian-Wei Wang for experimental assistance on magnetic measurements.

REFERENCES

(1) (a) Yamanouchi, M.; Chiba, D.; Matsukura, F.; Ohno, H. *Nature* **2004**, *428*, 539. (b) Saitoh, E.; Miyajima, H.; Yamaoka, T.; Tatara, G. *Nature* **2004**, *432*, 203. (c) Bogani, L.; Wernsdorfer, W. *Nat. Mater.* **2008**, *7*, 179. (d) Leuenberger, M. N.; Loss, D. *Nature* **2001**, *410*, 789. (e) Manoli, M.; Collins, A.; Parsons, S.; Candini, A.; Evangelisti, M.; Brechin, E. K. *J. Am. Chem. Soc.* **2008**, *130*, 11129. (f) Sessoli, R.; Gatteschi, D.; Caneschi, A.; Novak, M. A. *Nature* **1993**, *365*, 141. (g) Binnemans, K. *Coord. Chem. Rev.* **2009**, *109*, 4283. (h) Ward, M. D. *Coord. Chem. Rev.* **2007**, *251*, 1663.

(2) Atanasov, M.; Comba, P.; Hausberg, S.; Martin, B. *Coord. Chem. Rev.* **2009**, *253*, 2306.

(3) Cornia, A.; Mannini, M.; Sainctavit, P.; Sessoli, R. *Chem. Soc. Rev.* **2011**, *40*, 3076.

(4) (a) Katoh, K.; Isshiki, H.; Komeda, T.; Yamashita, M. *Coord. Chem. Rev.* **2011**, *255*, 2124. (b) Rinehart, J. D.; Long, J. R. *J. Am. Chem. Soc.* **2009**, *131*, 12558. (c) Lin, S.-Y.; Zhao, L.; Guo, Y.-N.; Zhan, P.; Guo, Y.; Tang, J.-K. *Inorg. Chem.* **2012**, *51*, 10522. (d) Freedman, D. E.; Harman, W. H.; Harris, T. D.; Long, G. J.; Chang, C. J.; Long, J. R. *J. Am. Chem. Soc.* **2010**, *132*, 1224. (e) Jiang, S.-D.; Liu, S.-S.; Zhou, L.-N.; Wang, B.-W.; Wang, Z.-M.; Gao, S. *Inorg. Chem.* **2012**, *51*, 3079. (f) Baldovi, J. J.; Cardona-Serra, S.; Clemente-Juan, J. M.; Coronado, E.; Gaita-Arino, A. *Chem. Sci.* **2013**, *4*, 938. (g) Suzuki, K.; Sato, R.; Mizuno, N. *Chem. Sci.* **2013**, *4*, 596. (h) Coutinho, J. T.; Antunes, M. A.; Pereira, L. C. J.; Bolvin, H.; Marcalo, J.; Mazzanti, M.; Almeida, M. *Dalton Trans.* **2012**, *41*, 13568. (i) Pointillart, F.; Bernot, K.; Poneti, G.; Sressoli, R. *Inorg. Chem.* **2012**, *51*, 12218. (j) Venugopal, A.; Tuna, F.; Spaniol, T. P.; Ungur, L.; Chibotaru, L. F.; Okuda, J.; Layfield, R. A. *Chem. Commun.* **2013**, *49*, 901. (k) Lin, P.-H.; Sun, W.-B.; Tian, Y.-M.; Yan, P.-F.; Ungur, L.; Chibotaru, L. F.; Murugesu, M. *Dalton Trans.* **2012**, *41*, 12349. (l) Wang, H.-L.; Cao, W.; Liu, T.; Duan, C.-Y.; Jiang, J.-Z. *Chem.—Eur. J.* **2013**, *19*, 2266. (m) Liu, S.-J.; Zhao, J.-P.; Song, W.-C.; Han, S.-D.; Liu, Z.-Y.; Bu, X.-H. *Inorg. Chem.* **2013**, *52*, 2103. (n) Pointillart, F.; Le Guennic, B.; Maury, O.; Golhen, S.; Cador, O.; Ouahab, L. *Inorg. Chem.* **2013**, *52*, 1398.

(5) Ishikawa, N.; Mizuno, Y.; Takamatsu, S.; Ishikawa, T.; Koshihara, S. *Inorg. Chem.* **2008**, *47*, 10217.

(6) Ishikawa, N.; Sugita, M.; Ishikawa, T.; Koshihara, S.; Kaizu, Y. *J. Am. Chem. Soc.* **2003**, *125*, 8694.

(7) (a) AlDamen, M. A.; Cardona-Serra, S.; Clemente-Juan, J. M.; Coronado, E.; Marti-Gastaldo, C.; Luis, F.; Montero, O. *Inorg. Chem.* **2009**, *48*, 3467. (b) AlDamen, M. A.; Clemente-Juan, J. M.; Coronado, E.; Marti-Gastaldo, C.; Gaita-Arino, A. *J. Am. Chem. Soc.* **2008**, *130*, 8874.

(8) Rinehart, J. D.; Long, J. R. *Chem. Sci.* **2011**, *2*, 2078.

(9) Yao, M.-X.; Zheng, Q.; Gao, F.; Li, Y.-Z.; Song, Y.; Zuo, J.-L. *Dalton Trans.* **2012**, *41*, 13682.

(10) (a) Zhu, X.-J.; Jiang, F.-L.; Poon, C.-T.; Wong, W.-K.; Wong, W.-Y. *Eur. J. Inorg. Chem.* **2008**, 3151. (b) Ke, H.-Z.; Wong, W.-K.; Wong, W.-Y.; Tam, H.-L.; Poon, C.-T.; Jiang, F.-L. *Eur. J. Inorg. Chem.* **2009**, 1243. (c) Foley, T. J.; Ha, B. S.; Knefely, S.; Abboud, K. A.; Reynolds, J. R.; Schanze, K. S.; Boncella, J. M. *Inorg. Chem.* **2003**, *42*, 5023.

(11) (a) Wong, W.-K.; Hou, A.-X.; Guo, J.-P.; He, H.-S.; Zhang, L.-L.; Wong, W.-Y.; Li, K.-F.; Cheah, K.-W.; Xue, F.; Mak, T. C. W. *J. Chem. Soc., Dalton Trans.* **2001**, 3092. (b) Zhu, X.-J.; Wang, P.; Leung, H. W. C.; Wong, W.-K.; Wong, W.-Y.; Kwong, D. W. J. *Chem.—Eur. J.* **2011**, *17*, 7041. (c) Jiang, F.-L.; Wong, W.-K.; Zhu, X.-J.; Zhou, G.-J.; Wong, W.-Y.; Wu, P.-L.; Tam, H.-L.; Cheah, K.-W.; Ye, C.; Liu, Y. *Eur. J. Inorg. Chem.* **2007**, 3365.

(12) Kläui, W.; Muller, A.; Eberspach, W.; Boese, R.; Goldbergs, I. *J. Am. Chem. Soc.* **1987**, *109*, 164.

(13) Boudreaux, E. A.; Mulay, L. N. *Theory and Application of Molecular Paramagnetism*; John Wiley & Sons: New York, 1976; p 491.

(14) *SAINT-Plus*, version 6.02; Bruker Analytical X-ray System: Madison, WI, 1999.

(15) Sheldrick, G. M. *SADABS, an empirical absorption correction program*; Bruker Analytical X-ray Systems: Madison, WI, 1996.

(16) Sheldrick, G. M. *SHELXTL-97*; Universität of Göttingen: Göttingen, Germany, 1997.
(17) (a) Girolami, G. S.; Milam, S. N.; Susllick, K. S. *Inorg. Chem.* **1987**, *26*, 343. (b) Kim, H.-J.; Whang, D.; Kim, K.; Do, Y. *Inorg. Chem.* **1993**, *32*, 360.
(18) Kahn, M. L.; Sutter, J. P.; Golhen, S.; Guionneau, P.; Ouahab, L.; Kahn, O.; Chasseau, D. *J. Am. Chem. Soc.* **2000**, *122*, 3413.
(19) Feng, W.-X.; Zhang, Y.; Zhang, Z.; Lü, X.-Q.; Liu, H.; Shi, G.-X.; Zou, D.; Song, J.-R.; Fan, D.-D.; Wong, W.-K.; Jones, R. A. *Inorg. Chem.* **2012**, *51*, 11377.
(20) Li, D.-P.; Zhang, X.-P.; Wang, T.-W.; Ma, B.-B.; Li, C.-H.; Li, Y.-Z.; You, X.-Z. *Chem. Commun.* **2011**, *47*, 6867.
(21) Tang, J.-K.; Hewitt, I.; Madhu, N. T.; Chastanet, G.; Wernsdorfer, W.; Anson, C. E.; Benelli, C.; Sessoli, R.; Powell, A. K. *Angew. Chem., Int. Ed.* **2006**, *45*, 1729.
(22) (a) Wang, H.-L.; Qian, K.; Wang, K.; Bian, Y.-Z.; Jiang, J.-Z.; Gao, S. *Chem. Commun.* **2011**, *47*, 9624. (b) Li, D.-P.; Wang, T.-W.; Li, C.-H.; Liu, D.-S.; Li, Y.-Z.; You, X.-Z. *Chem. Commun.* **2010**, *46*, 2929. (c) Jiang, S.-D.; Wang, B.-W.; Su, G.; Wang, Z.-M.; Gao, S. *Angew. Chem., Int. Ed.* **2010**, *49*, 7448. (d) Lin, P.-H.; Burchell, T. J.; Clerac, R.; Murugesu, M. *Angew. Chem., Int. Ed.* **2008**, *47*, 8848. (e) Vallejo, J.; Castro, I.; Garcia, R. R.; Cano, J.; Julve, M.; Lioret, F.; Munno, G. D.; Wernsdorfer, W.; Pardo, E. *J. Am. Chem. Soc.* **2011**, *134*, 15704. (f) Ishikawa, N.; Sugita, M.; Wernsdorfer, W. *J. Am. Chem. Soc.* **2005**, *127*, 3650. (g) Langley, S. K.; Chilton, N. F.; Ungur, L.; Moubaraki, B.; Chibotaru, L. F.; Murray, K. S. *Inorg. Chem.* **2012**, *51*, 11873. (h) Wang, H.-L.; Liu, T.; Wang, K.; Duan, C.-Y.; Jiang, J.-Z. *Chem.—Eur. J.* **2012**, *18*, 7691.
(23) Cole, K. S.; Cole, R. H. *J. Chem. Phys.* **1941**, *9*, 341.
(24) Ishii, N.; Okamura, Y.; Chiba, S.; Nogami, T.; Ishida, T. *J. Am. Chem. Soc.* **2008**, *130*, 24.
(25) Aubin, S. M.; Sun, Z.; Pardi, L.; Krzystek, J.; Folting, K.; Brunel, L. C.; Rheingold, A. L.; Christou, G.; Hendrickson, D. N. *Inorg. Chem.* **1999**, *38*, 5329.
(26) Katoh, K.; Horii, Y.; Yasuda, N.; Wernsdorfer, W.; Toriumi, K.; Breedlove, B. K.; Yamshita, M. *Dalton Trans.* **2012**, *41*, 13582.
(27) Long, J.; Habib, F.; Lin, P.-H.; Korobkov, I.; Enright, G.; Ungur, L.; Wensdorfer, W.; Chibotaru, L. F.; Murugesu, M. *J. Am. Chem. Soc.* **2011**, *133*, 5319.
(28) Jeletic, M.; Lin, P.-H.; Le Roy, J. J.; Korobkov, I.; Gorelsky, S. I.; Murugesu, M. *J. Am. Chem. Soc.* **2011**, *133*, 19286.
(29) Gonidec, M.; Luis, F.; Vilchez, A.; Esquena, J.; Amabilino, D. B.; Veciana, J. *Angew. Chem., Int. Ed.* **2010**, *49*, 1623.
(30) Luis, F.; Martinez-Perez, M. J.; Montero, O.; Coronado, E.; Cardona-Serra, S.; Marti-Gastaldo, C.; Clemente-Juan, J. M.; Sese, J.; Drung, D.; Schurig, T. *Phys. Rev. B* **2010**, 82.
(31) Katoh, K.; Kajiwara, T.; Nakano, M.; Nakazawa, Y.; Wernsdorfer, W.; Ishikawa, N.; Breedlove, B. K.; Yamashita, M. *Chem.—Eur. J.* **2011**, *17*, 117.
(32) Bi, Y.; Guo, Y.-N.; Zhao, L.; Guo, Y.; Lin, S.-Y.; Jiang, S.-D.; Tang, J.-K.; Wang, B.-W.; Gao, S. *Chem.—Eur. J.* **2011**, *17*, 12476.
(33) Watanable, A.; Yamashita, A.; Nakano, M.; Yamamura, T.; Kajiwara, T. *Chem.—Eur. J.* **2011**, *17*, 7428.
(34) Ishikawa, N.; Otsuka, S.; Kaizu, Y. *Angew. Chem., Int. Ed.* **2005**, *44*, 731.
(35) Gatteschi, D.; Sessoli, R. *Angew. Chem., Int. Ed.* **2003**, *115*, 278.
(36) Wernsdorfer, W.; Aliaga-Alcalde, N.; Hendrickson, D. N.; Christou, G. *Nature* **2002**, *416*, 408.